THE JOURNAL OF BIOLOGICAL CHEMISTRY VOL. 285, NO. 50, pp. 38898–38904, December 10, 2010

Subunit Symmetry at the Extracellular Domain-Transmembrane Domain Interface in Acetylcholine Receptor Channel Gating*

Received for publication, July 27, 2010, and in revised form, September 20, 2010 Published, JBC Papers in Press, September 23, 2010, DOI 10.1074/jbc.M110.169110

Iva Bruhova and Anthony Auerbach[1]

From the Department of Physiology and Biophysics, State University of New York at Buffalo, Buffalo, New York 14214

Transmitter molecules bind to synaptic acetylcholine receptor channels (AChRs) to promote a global channel-opening conformational change. Although the detailed mechanism that links ligand binding and channel gating is uncertain, the energy changes caused by mutations appear to be more symmetrical between subunits in the transmembrane domain compared with the extracellular domain. The only covalent connection between these domains is the pre-M1 linker, a stretch of five amino acids that joins strand β10 with the M1 helix. In each subunit, this linker has a central Arg ($Arg^{3'}$), which only in the non-α-subunits is flanked by positively charged residues. Previous studies showed that mutations of $Arg^{3'}$ in the α-subunit alter the gating equilibrium constant and reduce channel expression. We recorded single-channel currents and estimated the gating rate and equilibrium constants of adult mouse AChRs with mutations at the pre-M1 linker and the nearby residue Glu^{45} in non-α-subunits. In all subunits, mutations of $Arg^{3'}$ had similar effects as in the α-subunit. In the ε-subunit, mutations of the flanking residues and Glu^{45} had only small effects, and there was no energy coupling between ϵGlu^{45} and $\epsilon Arg^{3'}$. The non-α-subunit $Arg^{3'}$ residues had Φ-values that were similar to those for the α-subunit. The results suggest that there is a general symmetry between the AChR subunits during gating isomerization in this linker and that the central Arg is involved in expression more so than gating. The energy transfer through the AChR during gating appears to mainly involve Glu^{45}, but only in the α-subunits.

Acetylcholine receptors (AChRs)[2] are ligand-gated ion channels that mediate fast chemical synaptic transmission (1). The binding of two acetylcholine molecules to the extracellular domain (ECD) triggers a rapid, global, and reversible conformational change that increases the affinity of the two agonist-binding sites and opens a cation conduction pathway through the transmembrane domain (TMD). Defects in AChRs originating from inherited mutations that alter gating kinetic properties or expression cause myasthenic disorders (2). Electrophysiology studies have identified many mutations that produce abnormal AChR gating, but a detailed understanding of the mechanism by which the agonist affinity change and channel opening/closing are linked is not yet available.

The adult neuromuscular AChR consists of five homologous subunits (two α-subunits and one each of the β-, δ-, and ε-subunits) folded symmetrically around the central axis of the pore (3). Its structure is modular, as the extracellular N-terminal half of each subunit is a β-barrel and the transmembrane C-terminal half is a four-α-helix bundle (M1–M4). The five sets of β-barrels form the ECD, and the five sets of α-helices form the TMD. Several structures have revealed important features that are relevant to understanding the mechanism of energy transfer through the protein in the gating isomerization, including the *Torpedo* AChR (4), two prokaryotic pentameric ligand-gated ion channels crystallized in either a non-conducting (ELIC) (5) or a presumably conducting conformation (GLIC) (6, 7), an ECD fragment of the mouse AChR α-subunit (8), and the ECD homolog, the acetylcholine-binding protein (9). A comparison of the ELIC and GLIC x-ray structures suggests that the pore-lining M2 helices tilt tangentially and radially as part of the channel-opening process (6, 7). Despite this structural information, we are still unsure of the molecular events that constitute the affinity change at the binding sites and the conductance change at the pore or the intermediate events that couple structural changes in these two widely separated domains (10).

The interface between the ECD and TMD is a complex region that has been studied in several members of the Cys loop receptor channel family (11–18). This region has many charged residues and hence the potential for many non-bonded interactions. The only covalent link between the ECD and TMD is a stretch of five residues that join strand β10 with the M1 helix, known as the "pre-M1" linker (Fig. 1). This linker has a central positively charged Arg that is conserved among all pentameric ligand-gated receptor channels (12). Here, we will call this position $Arg^{3'}$ to mark it as the third position in this linker. Lee and Sine (12) proposed that the perturbation of a salt bridge between $\alpha Arg^{3'}$ and loop 2 residue αGlu^{45} is the principal event that links the ECD and the TMD in gating, but other results suggest that $\alpha Arg^{3'}$ plays a smaller role in gating but is important for receptor expression (14, 17).

The affinity change at the binding sites involves mainly α-subunit residues, but the opening and closing of the gate near the M2 equator involve the rearrangements of atoms in all five subunits. One goal of our experiments was to assay the symmetry of the gating energy changes at the pre-M1 linker, a location that is about halfway between the binding sites and the gate. In general, previous results indicate that large gating energy changes in the ECD are predominantly in the α-subunit but become more evenly spread among all subunits in the TMD (12,

* This work was supported, in whole or in part, by National Institutes of Health Grant NS-23513.

[1] To whom correspondence should be addressed: Dept. of Physiology and Biophysics, State University of New York at Buffalo, 309 Cary Hall, Buffalo, NY 14214. Tel.: 716-829-3450; Fax: 716-826-2569; E-mail: auerbach@buffalo.edu.

[2] The abbreviations used are: AChR, acetylcholine receptor channel; ECD, extracellular domain; TMD, transmembrane domain.

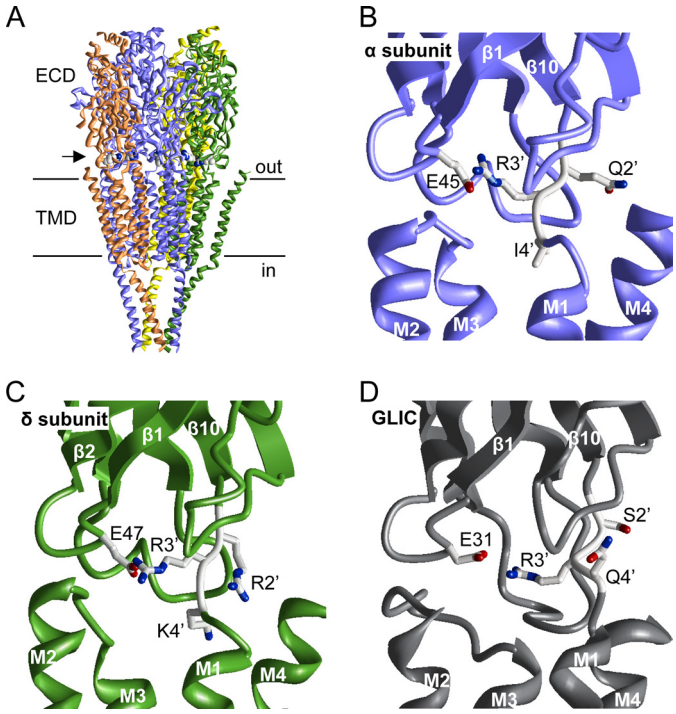

FIGURE 1. **Structure of the pre-M1 linker.** *A*, the cryo-EM structure of the *Torpedo* AChR (4). The *horizontal lines* mark approximately the membrane. The *arrow* points to the location of the pre-M1 linker. The $Arg^{3'}$ side chains of all subunits are space-filled. *B* and *C*, close-up view of the pre-M1 linker of the α- and δ-subunits in the *Torpedo* AChR. The side chains of a Glu in loop 2 and pre-M1 linker positions 2′, 3′, and 4′ are shown as *sticks*, where carbons, oxygens, and nitrogens are colored *gray*, *red*, and *blue*, respectively. The backbones of the ECD, TMD, and loops are displayed as *smooth ribbons*, *flat ribbons*, and *rods*, respectively. *D*, close-up view of the pre-M1 linker of GLIC (7). Structures were displayed using MVM (ZMM Software Inc.).

19–25). Although the mechanism of this spreading of the gating energy changes is not clear, an intersubunit energy transfer has been found between αTyr^{127} and ϵAsn^{39} or δAsn^{41} (19).

So far, only one mutation at one pre-M1 linker position has been studied in all subunits using single-channel kinetic analysis. A Gln substitution at the fourth linker residue modestly increases diliganded gating (by ~3-fold) in the α-subunit but is without effect in the non-α-subunits (26). Here, we report the effects of mutations of multiple pre-M1 residues in non-α-subunits, estimated from the single-channel rate and equilibrium constants of the adult mouse AChR gating isomerization.

EXPERIMENTAL PROCEDURES

Mutagenesis and Expression—A detailed description of our methods is described by Jha *et al.* (27). Mutant AChR cDNAs were made by QuikChange™ site-directed mutagenesis (Stratagene) and confirmed by sequencing. We made 26 mutants of the ϵ-subunit, three double-mutant combinations of the ϵ-subunit, two mutants of the β-subunit, and two mutants of the δ-subunit. HEK293 cells were transiently transfected by the calcium phosphate precipitation method. HEK cells were incubated with 2.5–5 μg of mouse WT or mutant cDNAs in a 35-mm culture dish at a subunit ratio of 2:1:1:1 (α/β/δ/ϵ). After ~16 h of incubation at 37 °C, the transfected cells were washed with HEK culture medium. Electrophysiology recordings were performed 20–40 h post-transfection.

TABLE 1

Sequence alignment of the pre-M1 linker

The conserved central Arg at position 3′ is shown in boldface: αArg^{209}, βArg^{220}, δArg^{223}, and ϵArg^{218} in mouse AChR numbering.

Protein	Positions 1–5′
Mouse AChR	
α-subunit	MQ**R**LP
α_2-subunit	IR**R**LP
α_3-subunit	IR**R**LP
α_4-subunit	IR**R**LP
α_5-subunit	IK**R**LP
α_6-subunit	IR**R**LP
α_7-subunit	MR**R**RT
β-subunit	IR**R**KP
β_2-subunit	IR**R**KP
β_3-subunit	LR**R**LP
β_4-subunit	IK**R**KP
δ-subunit	IR**R**KP
ϵ-subunit	IR**R**KP
γ-subunit	IQ**R**KP
***Torpedo* AChR α-subunit**	MQ**R**IP
ELIC	AV**R**NP
GLIC	IS**R**QY

Single-channel Recordings and Kinetic Analysis—Recordings were carried out in the cell-attached patch configuration at room temperature (23 °C). The pipette and bath solutions were both Dulbecco's PBS (137 mM NaCl, 0.9 mM $CaCl_2$, 2.7 mM KCl, 1.5 mM KH_2PO_4, 0.5 mM $MgCl_2$, and 8.1 mM Na_2HPO_4 at pH 7.2). Pipettes were pulled from borosilicate capillaries to a resistance of ~10 megohms and coated with SYLGARD (Dow Corning Corp., Midland, MI). The pipette solution contained 0.5 mM acetylcholine, 20 mM choline, or 5 mM carbamylcholine. These agonist concentrations are approximately five times the corresponding equilibrium dissociation constants (K_d); thus, almost all currents arose from diliganded AChRs. Because the mutations were far from the binding site, we assumed that they did not change K_d. The high concentration of agonist caused partial channel block, which decreases both the apparent single-channel current amplitude and the apparent closing rate constant. Although none of the mutations changed the degree of channel block, nonetheless we measured the closing rate constant using low concentrations of agonist (30 μM acetylcholine, 200 μM choline, and 200 μM carbamylcholine), at which channel block is insignificant. The diliganded gating equilibrium constant (E_2) was calculated as the ratio of the opening/closing rate constant. Choline was used to measure the diliganded opening rate constant for AChR mutants where E_2 was larger than or equal to the WT; acetylcholine was used for mutants where E_2 was less than the WT; and carbamylcholine was used to measure mutants where E_2 was approximately equal to the WT. It has been shown for many non-binding site mutations that different agonists support the same Φ-values and fold-changes in E_2 (21).

Cells were held at a pipette potential of +70 mV, which corresponds to a membrane potential of approximately −100 mV. Errors in the rate constants associated with the errors in the membrane voltage are small (in WT AChRs, an ~70-mV depolarization is necessary to decrease E_2 by *e*-fold) (28). Currents were filtered at 20 kHz and digitized at a sampling frequency of 50 kHz. Kinetic analyses were done using QUB software. Currents were idealized using the SKM (segmental K-Means) algorithm filtered at 12 kHz with a C ↔ O (closed ↔ open) model

with starting rate constants of 100 s^{-1}. The diliganded opening (f_2) and closing (b_2) rate constants were estimated from idealized interval durations using a maximum interval likelihood algorithm after incorporating a dead time of 25 μs (29).

The diliganded rate constants were measured multiple times (n = two to five patches) and then averaged. Φ was estimated as the slope of the linear fit to the log-log rate-equilibrium free energy relationship (R/E analysis). The range energy (kcal/mol) = $-0.59 \ln(E_2^{max}/E_2^{min})$, where the superscripts are the E_2 values for the side chains generating the largest and smallest E_2 values, respectively. The coupling free energy was calculated as $\Delta\Delta G$ (kcal/mol) = $-0.59 \ln((E_{double\ mutant})/(E_{mutant\ 1}{}^{*}E_{mutant\ 2}))$.

RESULTS

ϵ-Subunit Linker—Table 1 shows a sequence alignment of the pre-M1 linker and that $Arg^{3'}$ is completely conserved. In the α-subunit linker, this is the only positively charged residue, but in the non-α-subunits, it is flanked by two additional basic amino acids.

We estimated residue range energy (see "Experimental Procedures") and Φ-values from AChRs with a mutation of one of the three positively charged amino acids in the ϵ-linker ($\epsilon Arg^{2'}$, $\epsilon Arg^{3'}$, $\epsilon Lys^{4'}$). None of the side chain substitutions at $\epsilon Arg^{2'}$ (Ala, Cys, Asp, Asn, Trp, or Val) changed the diliganded gating equilibrium constant (E_2) by >2-fold (Fig. 2 and Table 2). This set of substitutions was selected to include residues of different size, charge, and hydrophobicity. All mutations caused a slight reduction in E_2, with the largest being for Asn (1.8-fold, which corresponds to a range energy of 0.3 kcal/mol). We conclude that like its homolog in the α-subunit, the $\epsilon 2'$-side chain is nearly isoenergetic between the ground state conformations, which suggests that this amino acid does not move with respect to its local environment during the gating isomerization.

Nine substitutions of the central position $\epsilon Arg^{3'}$ were examined, but only Ala, His, Lys, Asn, and Gln expressed functional channels. We were unable to observe single-channel currents from the Cys, Asp, Glu, and Val mutants (3–10 patches per mutant, recording for 15–25 min/patch). In this respect, position $\epsilon 3'$ behaves similarly to its homolog in the α-subunit (14) and to $\alpha_1 Arg^{220}$ in the GABA receptor channel (17), where mutations also reduce the expression of functional channels. Mutations of $\epsilon Arg^{3'}$ had substantial effects on E_2 (Table 2). The Ala, His, Lys, Asn, and Gln substitutions all decreased E_2 compared with the

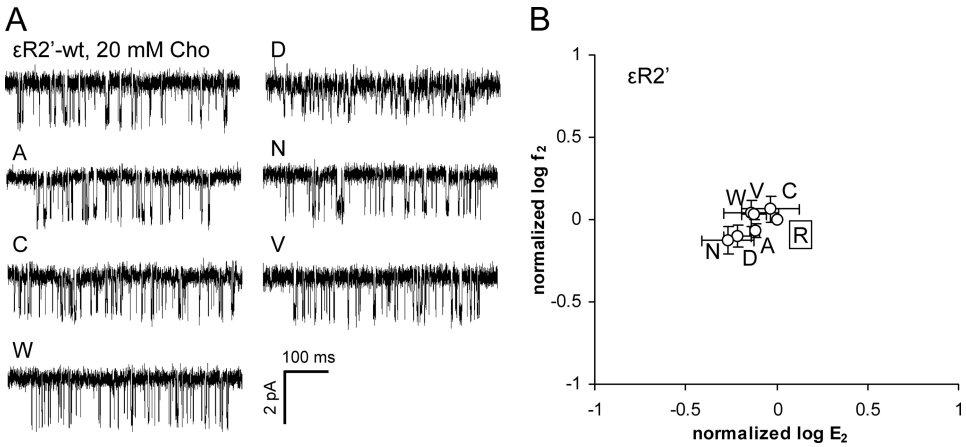

FIGURE 2. **Mutations of $\epsilon Arg^{2'}$ (ϵArg^{217}) have little effect on the gating equilibrium constant.** The small change in the diliganded gating equilibrium constant (E_2, normalized by the WT value) indicates that this position is nearly isoenergetic between the ground state conformations. *A*, example clusters elicited by 20 mM choline (*Cho*). *B*, *R/E* analysis. Each *point* represents the average of three patches with its S.D. (Table 2). The WT is *boxed*.

TABLE 2

Kinetic parameters for ϵ-subunit pre-M1 mutants

The investigated ϵ-subunit pre-M1 positions studied were $\epsilon Arg^{2'}$, $\epsilon Arg^{3'}$, and $\epsilon Lys^{4'}$, which in the mouse AChR are numbered ϵArg^{217}, ϵArg^{218}, and ϵLys^{219}, respectively. The numbers are the mean ± S.D. ACh, acetylcholine; Cho, choline; f_2, forward (opening) rate constant; b_2^{obs}, observed backward (closing) rate constant; b_2^{cor}, backward rate constant corrected for channel block; E_2, diliganded gating equilibrium constant (calculated as f_2/b_2^{cor}); n, number of patches. Normalized values are mutant/WT. No single-channel currents were observed with ϵR3′C, ϵR3′D, ϵR3′E, and ϵR3′V mutants.

Construct	Agonist[a]	f_2	b_2^{obs}	b_2^{cor}	E_2 (f_2/b_2^{cor})	Normalized f_2 (mutant/WT)	Normalized E_2 (mutant/WT)	n
		s^{-1}	s^{-1}	s^{-1}				
WT[b]	ACh	48,000		1750	28.00	1.00	1.00	
WT	Cho	120		2583	0.05	1.00	1.00	
ϵR2′A	Cho	104 ± 10	783 ± 88	2934 ± 329	0.04 ± 0.002	0.86	0.76	3
ϵR2′C	Cho	139 ± 24	933 ± 202	3232 ± 700	0.05 ± 0.02	1.16	0.97	3
ϵR2′D	Cho	95 ± 15	869 ± 60	3372 ± 235	0.03 ± 0.01	0.79	0.61	3
ϵR2′N	Cho	90 ± 17	849 ± 217	3586 ± 918	0.03 ± 0.01	0.75	0.56	3
ϵR2′W	Cho	131 ± 24	1247 ± 209	3891 ± 652	0.04 ± 0.01	1.09	0.76	3
ϵR2′V	Cho	129 ± 10	896 ± 109	3719 ± 454	0.04 ± 0.01	1.08	0.76	3
ϵR3′A	ACh	991 ± 171	4397 ± 826	6572 ± 1234	0.15 ± 0.02	0.02	0.005	3
ϵR3′H	ACh	9019 ± 1907	2623 ± 648	6194 ± 1530	1.56 ± 0.63	0.19	0.055	3
ϵR3′K	ACh	6363 ± 856	2579 ± 261	4627 ± 468	1.40 ± 0.29	0.13	0.050	4
ϵR3′N	ACh	1559 ± 159	6813 ± 980	10,311 ± 1484	0.15 ± 0.04	0.03	0.006	3
ϵR3′Q	ACh	1446 ± 35	3180 ± 840	5726 ± 1513	0.27 ± 0.07	0.03	0.009	4
ϵK4′A	Cho	325 ± 56	431 ± 76	1634 ± 286	0.20 ± 0.03	2.71	4.31	3
ϵK4′C	Cho	300 ± 60	712 ± 251	2327 ± 820	0.15 ± 0.08	2.50	3.14	3
ϵK4′D	Cho	221 ± 20	593 ± 46	2260 ± 174	0.10 ± 0.01	1.84	2.11	3
ϵK4′N	Cho	111 ± 8	525 ± 141	2213 ± 596	0.05 ± 0.01	0.93	1.12	3
ϵK4′W	Cho	351 ± 36	351 ± 25	1099 ± 79	0.32 ± 0.03	2.92	6.87	3
ϵK4′V	Cho	135 ± 20	706 ± 43	2600 ± 158	0.05 ± 0.01	1.12	1.12	3

[a] Agonist concentration was ~5-fold the equilibrium dissociation constant (0.5 mM acetylcholine or 20 mM choline).
[b] Wild-type constants for acetylcholine and choline were taken from Chakrapani and Auerbach (32) and Mitra *et al.* (24), respectively.

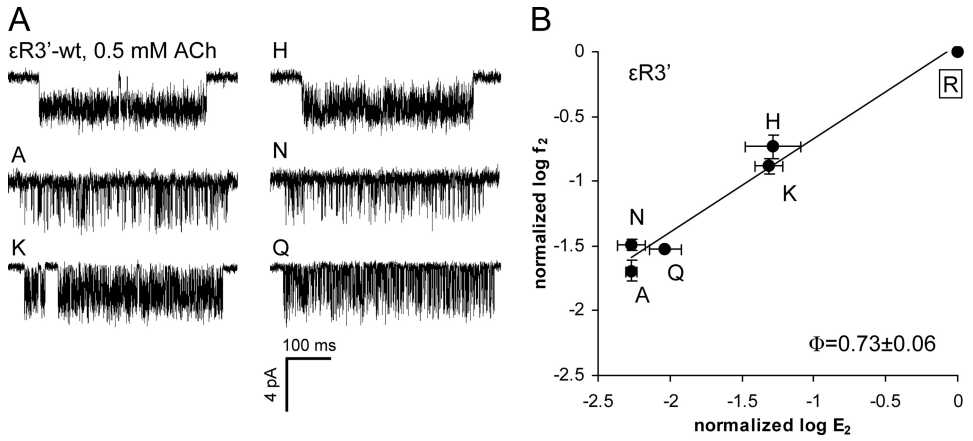

FIGURE 3. **Mutations of $\epsilon Arg^{3'}$ (ϵArg^{218}) decrease the gating equilibrium constant.** *A*, example clusters elicited by 0.5 mM acetylcholine (*ACh*). Single-channel currents were not detected for the Cys, Asp, Glu, Val, and Trp mutants. *B*, *R/E* analysis. Each *point* represents the average of three to four patches with its S.D. (Table 2). ●, acetylcholine-activated. The WT is *boxed*. The Φ-value (*lower right*) was estimated as the linear slope of log f_2 *versus* log E_2 and gives the relative timing of the residue's gating energy change (1 to 0, start to end). The $\epsilon Arg^{3'}$ side chain changes its energy relatively early in the channel-opening process.

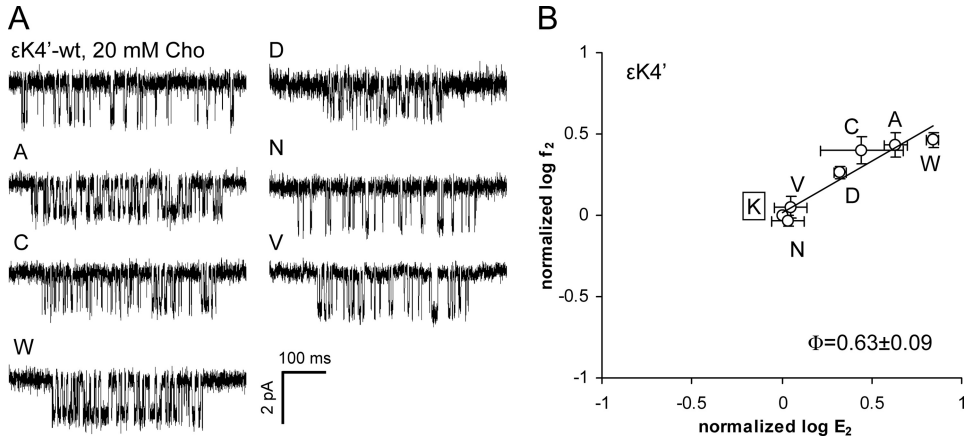

FIGURE 4. **Mutations of $\epsilon Lys^{4'}$ (ϵLys^{219}) modestly increase the gating equilibrium constant.** *A*, example clusters activated by 20 mM choline (*Cho*). *B*, *R/E* analysis. Each *point* represents the average of three patches with its S.D. (Table 2). The WT is *boxed*. The Φ-value (*lower right*) was estimated as the linear slope of log f_2 *versus* log E_2.

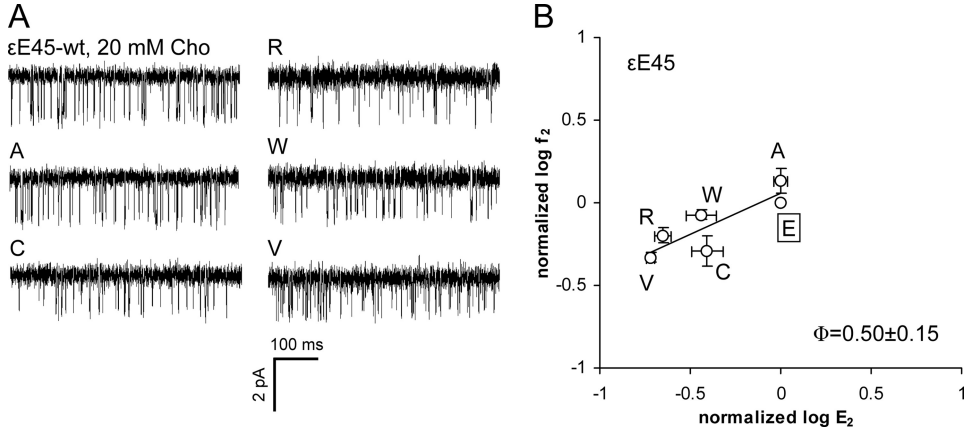

FIGURE 5. **Mutations of ϵGlu^{45} have only a small effect on the gating equilibrium constant.** *A*, example clusters activated by 20 mM choline (*Cho*). *B*, *R/E* analysis. Each *point* represents the average of two to three patches with its S.D. (Table 3). The WT is *boxed*. The Φ-value (*lower right*) was estimated as the linear slope of log f_2 *versus* log E_2.

WT (Fig. 3). The Ala and Asn substitutions had the largest effect and decreased E_2 by ~180-fold. The range energy for $\epsilon Arg^{3'}$ was ~3.1 kcal/mol, which is about the median value for two α-subunit mutations (10, 30). The *R/E* plot for $\epsilon Arg^{3'}$ had a slope (Φ-value) of 0.73 ± 0.06 (Fig. 3*B*), which indicates that the change in E_2 was caused mainly by a reduction in the forward channel-opening rate constant (f_2). This Φ-value is the same as for $\alpha Arg^{3'}$ (14), which suggests that the central Arg residues experience a change in energy at about the same time in the gating reaction in the α- and ε-subunits.

All substitutions tested at $\epsilon Lys^{4'}$ expressed functional AChRs. Ala, Cys, Asp, and Trp mutations increased E_2, but only modestly (Fig. 4 and Table 2). The Trp mutant showed the largest energy change (~1.1 kcal/mol). AChRs with an Asn or Val side chain here had WT gating properties, as did a Gln substitution (26). The Φ-value of the $\epsilon Lys^{4'}$ series was 0.63 ± 0.09, similar to that of its neighbor $\epsilon Arg^{3'}$. However, in the α-subunit, the Φ-value of $\alpha Leu^{4'}$ (Φ = 0.35) was distinctly lower than that of the adjacent residue $\alpha Arg^{3'}$ (Φ = 0.72) (14).

Energetic Coupling between $\epsilon Arg^{3'}$ and ϵGlu^{45}—In the cryo-EM structure of the *Torpedo* AChR (4), the positively charged side chain of $\alpha Arg^{3'}$ faces the negatively charged side chain of αGlu^{45}, and swapping charges here restores functional gating (12). We investigated the effects of five side chain substitutions at ϵGlu^{45} and three ϵGlu^{45}/$\epsilon Arg^{3'}$ double-mutant combinations to explore the interactions between these ε-positions during gating.

Fig. 5 and Table 3 show the effects of mutating ϵGlu^{45}. The ϵGlu^{45} substitutions Cys, Arg, Trp, and Val all decreased E_2, but only slightly (<1 kcal/mol). The Φ-value measured for the ϵGlu^{45} mutation series was 0.50 ± 0.15. Because of the near-WT gating properties of the εE45A mutant, we conclude that a negatively charged side chain at this position in the ε-subunit is not critical for efficient gating. The small range energy makes the ϵGlu^{45} Φ-value estimate imprecise (31), but it may be that this residue changes its energy somewhat after its α-subunit homolog (Φ = 0.80) (14).

TABLE 3

Kinetic parameters for ϵGlu^{45} mutants

See the legend to Table 2. No single-channel currents were observed with the ϵR3′E/ϵE45R double mutant. Cho, choline; ACh, acetylcholine.

Construct	Agonist	f_2	b_2^{obs}	b_2^{cor}	E_2 (f_2/b_2^{cor})	Normalized E_2 (mutant/WT)		$\Delta\Delta G$	n
						Observed	Predicted		
		s^{-1}	s^{-1}	s^{-1}				*kcal/mol*	
ϵE45A	Cho	164 ± 27	1238 ± 112	3519 ± 319	0.05 ± 0.004	1.01			3
ϵE45C	Cho	61 ± 13	1041 ± 26	3365 ± 83	0.02 ± 0.004	0.40			3
ϵE45R	Cho	56 ± 4	1551 ± 74	6321 ± 301	0.01 ± 0.001	0.19			3
ϵE45W	Cho	102 ± 7	1156 ± 141	6032 ± 733	0.02 ± 0.003	0.37			2
ϵE45V	Cho	76 ± 8	2443 ± 1	7404 ± 1	0.01 ± 0.001	0.22			2
ϵR3′Q/ϵE45A	ACh	2258 ± 382	3219 ± 521	5631 ± 911	0.41 ± 0.10	0.015	0.009	−0.30	5
ϵR3′K/ϵE45A	Cho	38 ± 12	1076 ± 181	3986 ± 669	0.01 ± 0.01	0.216	0.050	−0.86	4

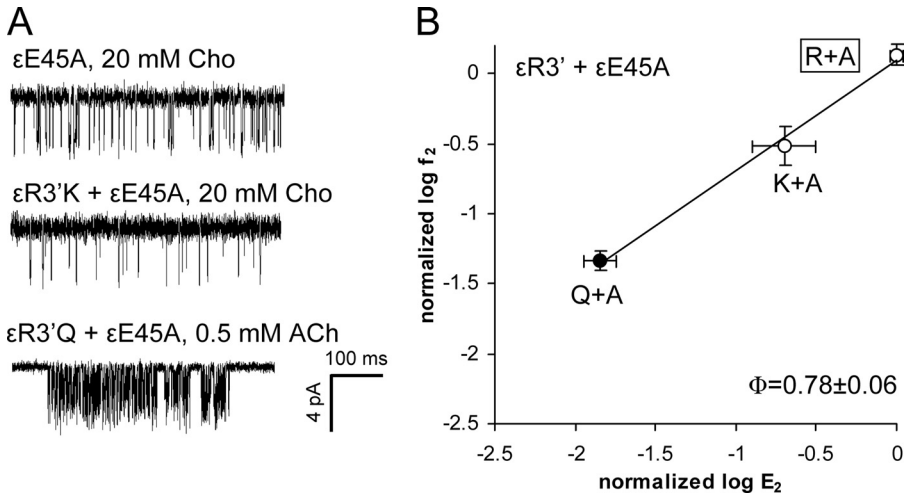

FIGURE 6. **Energy coupling between $\epsilon Arg^{3'}$ and ϵGlu^{45}.** *A*, example clusters activated by different agonists. *B*, *R/E* analysis. Each *point* represents the average of three to five patches with its S.D. (Table 4). ●, acetylcholine (*ACh*); ○, choline (*Cho*). The WT is *boxed*. The Φ-value (*lower right*) was estimated as the linear slope of log f_2 *versus* log E_2.

We created three $\epsilon Glu^{45}/\epsilon Arg^{3'}$ double-mutant constructs: Arg/Glu, Ala/Gln, and Ala/Lys. In the α-subunit, the side chains of αGlu^{45} influence the expression of $\alpha Arg^{3'}$ mutants (14). The ϵR3′E construct alone did not express functional AChRs, and when we expressed this along with ϵE45R (a charge swap), we still did not observe the expression of functional AChRs currents. The other two double-mutant pairs (Ala/Gln and Ala/Lys) did express functional channels and produced AChRs having slightly larger E_2 values than predicted assuming independence (Fig. 6 and Table 3). The Ala/Gln and Ala/Lys double mutants exhibited very small coupling energies (−0.3 and −0.9 kcal/mol, respectively). The *R*/*E* plot for $\epsilon Arg^{3'}$ on the ϵE45A background yielded a Φ-value of 0.78 ± 0.06 (Fig. 6*B*), which is similar to its value on the WT background (Fig. 3).

β- and δ-Subunit Linkers—We also examined the kinetics of mutations at position 3′ in the β- and δ-subunits (Fig. 7 and Table 4). The mutation βR3′K had little effect on gating, whereas a Gln mutation here resulted in a 49-fold reduction of E_2. The estimated Φ-value of position β3′ was 0.44 ± 0.06 (Fig. 7*B*). In the δ-subunit, Lys and Gln substitutions were assayed using two different agonists, acetylcholine and carbamylcholine. With both $\delta Arg^{3'}$ mutations, the fold-changes in E_2 were similar for these ligands, even though acetylcholine is a full agonist and carbamylcholine is a partial agonist. The *R*/*E* plot for position δ3′ yielded a Φ-value of 0.54 ± 0.07 and a range energy of ~2.0 kcal/mol.

DISCUSSION

In the *Torpedo* AChR (4) structure, the $\alpha Arg^{3'}$ side chain forms a salt bridge with αGlu^{45} in loop 2 (and possibly with αGlu^{175} in loop 9). In the ECD fragment of the mouse nicotinic acetylcholine receptor α-subunit (8), $\alpha Arg^{3'}$ interacts indirectly with αGlu^{45} via a structural water. An electrostatic contact is present between the $Arg^{3'}$ and Glu^{31} (in loop 2) side chains in the x-ray structure of GLIC (7). ELIC lacks this salt bridge because the loop 2 residue is a Thr that faces, but does not contact, $Arg^{3'}$ (which does appear to form a salt bridge with Asp^{122} in loop 7 and Glu^{159} in loop 9). Thus, the conserved pre-M1 linker $Arg^{3'}$ side chain is evidently involved in protein stability through electrostatic interactions with surrounding loops. However, analyses of function suggest that a perturbation of the salt bridge between $\alpha Arg^{3'}$ and αGlu^{45} is not a critically important event in AChR gating (14).

One of our goals was to probe the degree of functional symmetry between subunits with regard to residues in the pre-M1 linker and loop 2. The non-α-linker contains three positive residues, whereas the α-linker contains only one. Recall that in the α-subunit linker, (i) many mutations at position 3′ reduce expression, (ii) only mutations at positions 3′ and 4′ affect E_2, and (iii) loop 2 residue αGlu^{45} experiences a very large range energy change (~5 kcal/mol) early in the channel-opening process (Φ ~ 0.8) (14). We can compare this basic pattern in the α-subunit with that we have found in the ε-subunit and, to a lesser extent, in the β- and δ-subunits.

Position 2′ is isoenergetic in both the α- and ε-subunits. All mutants tested here in both subunits expressed functional AChRs that had WT-like currents. It appears that in the mouse AChR, this position in the pre-M1 linker in the α- and ε-subunits is not essential for folding, expression, conductance, gating, or desensitization.

Position 3′ is much more interesting. In both the α- and ε-subunits, many substitutions here prevented the expression of functional AChRs. Single-channel currents were observed

only with the Arg, Gln, His, and Lys side chains in both the α- and ϵ-subunits and also with Ala and Asn only in the ϵ-subunit. This difference in expression may simply reflect the fact that each AChR has two α-subunits but only one ϵ-subunit. The R3′Q substitution resulted in a reduction of E_2 in both α-subunits and all non-α-subunits, but the gating energy change was only moderate. The range energy (per subunit) was slightly larger in the ϵ-subunit (~3 kcal/mol) compared with the α-subunit (~2 kcal/mol); this result was influenced by the inclusion of the Ala and Asn substitutions only in the ϵ-subunit. Limiting this estimate to the Arg, Gln, His, and Lys side chains, the range energies were 1.8 and 1.0 kcal/mol/subunit for the α- and ϵ-subunits, respectively. The Φ-value for position 3′ was the same in the α- and ϵ-subunits, but those in the β- and δ-subunits were somewhat smaller. Overall, this pattern for the central pre-M1 linker position suggests that this region is approximately symmetric between subunits with regard to protein expression and the magnitude and relative timing of the gating energy changes. However, a Lys substitution at $Arg^{3'}$ resulted in an E_2 increase in the α-subunits but a decrease in the δ- and ϵ-subunits and no change in the β-subunit, suggesting that the α-subunit may have a unique chemical environment near the pre-M1 linker.

Position 4′ is not conserved between the α- and ϵ-subunits (Leu *versus* Lys), and this residue behaved quite differently in these two subunits. The αL4′K mutation increased E_2 by ~50-fold, whereas the ϵK4′V mutation (Leu was not tested) had no effect. Indeed, only small changes were observed for all tested mutations of $\epsilon Lys^{4'}$, whereas all mutations in the α-subunit modestly increased E_2 (range energy of ~2.3 kcal/mol). An even more interesting difference is the distinct Φ-values for position 4′ in the α-subunit *versus* the ϵ-subunit (0.35 *versus* 0.63). This suggests that in the α-subunit, but not the ϵ-subunit, there is a boundary between pre-M1 linker positions 3′ and 4′ that defines the relative timing of the gating movements of the ECD and TMD.

The gating behavior of loop 2 residue Glu^{45} was also very different in the α-subunit compared with the ϵ-subunit. Substitutions in the ϵ-subunit decreased E_2 very slightly, whereas those in the α-subunit either increased or decreased E_2 substantially. Indeed, the αGlu^{45} range energy (~5 kcal/mol, His to Ile) is the third largest measured so far in the ECD (after αAla^{96} and αTyr^{127}) (30). An important and common feature shared by Glu^{45} in

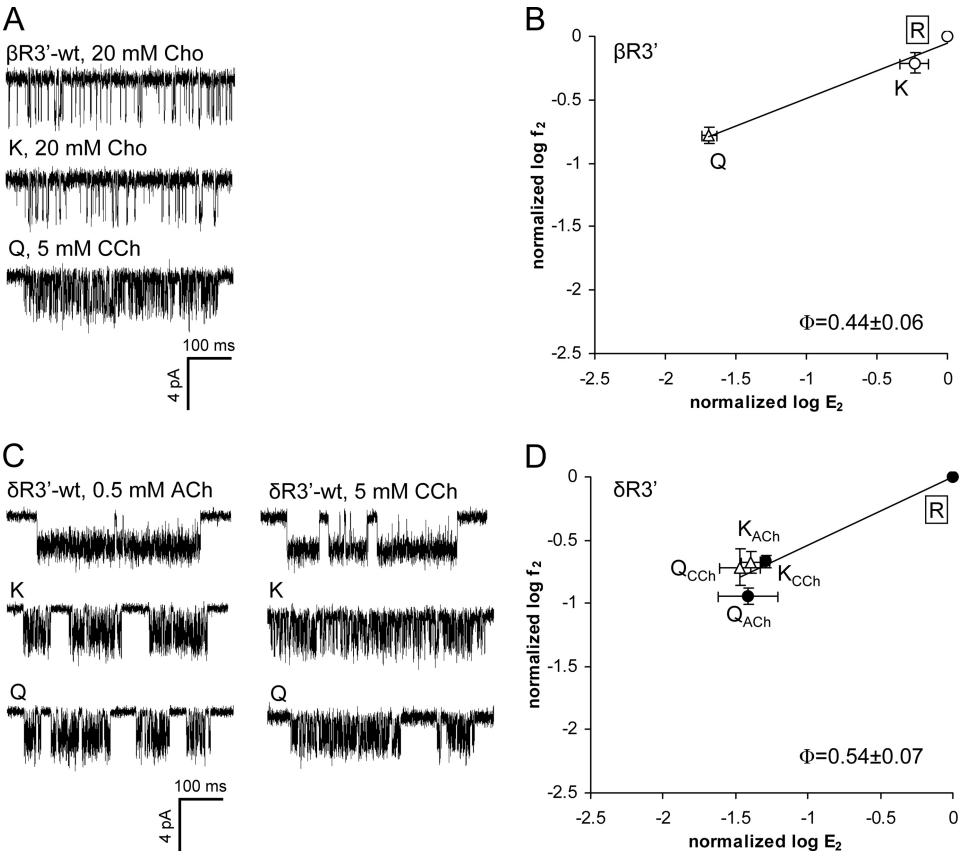

FIGURE 7. **Mutations of $\beta Arg^{3'}$ (βArg^{220}) and $\delta Arg^{3'}$ (δArg^{223}) decrease the diliganded gating equilibrium constant.** *A* and *C*, example clusters of position β3′ and δ3′ mutants activated by 0.5 mM acetylcholine (*ACh*), 5 mM carbamylcholine (*CCh*), or 20 mM choline (*Cho*). In *C*, the *left* clusters were activated by acetylcholine and the *right* clusters by carbamylcholine. *B* and *D*, *R/E* analyses of positions β3′ and δ3′ mutants. Each *point* represents the average of three to four patches with its S.D. (Table 4). ●, acetylcholine; ○, choline; △, carbamylcholine. The WT is *boxed*. The Φ-value (*lower right*) was estimated as the linear slope of log f_2 *versus* log E_2.

TABLE 4

Kinetic parameters for $\beta Arg^{3'}$ and $\delta Arg^{3'}$ positions

$\beta Arg^{3'}$ and $\delta Arg^{3'}$ are numbered in the mouse AChR as βArg^{220} and δArg^{223}, respectively. See the legend to Table 2. CCh, carbamylcholine; Cho, choline; ACh, acetylcholine.

Construct	Agonist	f_2	b_2^{obs}	b_2^{cor}	E_2 (f_2/b_2^{cor})	Normalized f_2 (mutant/WT)	Normalized E_2 (mutant/WT)	*n*
		s^{-1}	s^{-1}	s^{-1}				
WT[a]	CCh	7721		1138	6.80	1.00	1.00	
βR3′K	Cho	75 ± 14	769 ± 33	2709 ± 116	0.03 ± 0.01	0.62	0.60	4
βR3′Q	CCh	1290 ± 188	2586 ± 497	9300 ± 1789	0.14 ± 0.02	0.17	0.02	3
δR3′K	ACh	10,315 ± 1170	4668 ± 547	7271 ± 852	1.42 ± 0.10	0.21	0.05	4
δR3′Q	ACh	5462 ± 801	3341 ± 1502	5362 ± 2411	1.16 ± 0.48	0.11	0.04	4
δR3′K	CCh	1646 ± 318	1797 ± 650	6137 ± 2220	0.28 ± 0.04	0.21	0.04	3
δR3′Q	CCh	1553 ± 492	2656 ± 667	6644 ± 1668	0.24 ± 0.07	0.20	0.03	4

[a] WT rate constants for carbamylcholine were taken from Purohit and Auerbach (21).

the α- and ϵ-subunits is that double mutants of $Arg^{3'}$ and Glu^{45} in both subunits suggest weak energetic interactions between these side chains in gating.

In summary, the pre-M1 linker is mostly symmetrical between subunits at positions 2′ and 3′ with regard to expression, gating, and interactions with Glu^{45} in loop 2. Asymmetry between subunits was apparent at pre-M1 linker position 4′ and Glu^{45}, where only the α-subunit plays a major role. It is of interest to identify the chemical details that define the distinct subunit environments at the ECD-TMD interface and to further explore how energy spreads between subunits in the AChR gating isomerization.

Acknowledgments—We thank Mary Merritt for technical assistance and Archana Jha and Prasad Purohit for helpful discussions.

REFERENCES

1. Hille, B. (2001) *Ion Channels of Excitable Membranes*, 3rd Ed., Sinauer Associates, Inc., Sunderland, MA.
2. Engel, A. G., Shen, X. M., Selcen, D., and Sine, S. M. (2010) *J. Mol. Neurosci.* **40,** 143–153
3. Unwin, N. (1998) *J. Struct. Biol.* **121,** 181–190
4. Unwin, N. (2005) *J. Mol. Biol.* **346,** 967–989
5. Hilf, R. J., and Dutzler, R. (2008) *Nature* **452,** 375–379
6. Bocquet, N., Nury, H., Baaden, M., Le Poupon, C., Changeux, J. P., Delarue, M., and Corringer, P. J. (2009) *Nature* **457,** 111–114
7. Hilf, R. J., and Dutzler, R. (2009) *Nature* **457,** 115–118
8. Dellisanti, C. D., Yao, Y., Stroud, J. C., Wang, Z. Z., and Chen, L. (2007) *Nat. Neurosci.* **10,** 953–962
9. Brejc, K., van Dijk, W. J., Klaassen, R. V., Schuurmans, M., van Der Oost, J., Smit, A. B., and Sixma, T. K. (2001) *Nature* **411,** 269–276
10. Auerbach, A. (2010) *J. Physiol.* **588,** 573–586
11. Tamamizu, S., Todd, A. P., and McNamee, M. G. (1995) *Cell. Mol. Neurobiol.* **15,** 427–438
12. Lee, W. Y., and Sine, S. M. (2005) *Nature* **438,** 243–247
13. Xiu, X., Hanek, A. P., Wang, J., Lester, H. A., and Dougherty, D. A. (2005) *J. Biol. Chem.* **280,** 41655–41666
14. Purohit, P., and Auerbach, A. (2007) *J. Gen. Physiol.* **130,** 559–568
15. Hu, X. Q., Zhang, L., Stewart, R. R., and Weight, F. F. (2003) *J. Biol. Chem.* **278,** 46583–46589
16. Kash, T. L., Dizon, M. J., Trudell, J. R., and Harrison, N. L. (2004) *J. Biol. Chem.* **279,** 4887–4893
17. Mercado, J., and Czajkowski, C. (2006) *J. Neurosci.* **26,** 2031–2040
18. Castaldo, P., Stefanoni, P., Miceli, F., Coppola, G., Del Giudice, E. M., Bellini, G., Pascotto, A., Trudell, J. R., Harrison, N. L., Annunziato, L., and Taglialatela, M. (2004) *J. Biol. Chem.* **279,** 25598–25604
19. Mukhtasimova, N., and Sine, S. M. (2007) *J. Neurosci.* **27,** 4110–4119
20. Chakrapani, S., Bailey, T. D., and Auerbach, A. (2003) *J. Gen. Physiol.* **122,** 521–539
21. Purohit, P., and Auerbach, A. (2007) *J. Gen. Physiol.* **130,** 569–579
22. Grosman, C., Salamone, F. N., Sine, S. M., and Auerbach, A. (2000) *J. Gen. Physiol.* **116,** 327–340
23. Bafna, P. A., Purohit, P. G., and Auerbach, A. (2008) *PLoS One* **3,** e2515
24. Mitra, A., Cymes, G. D., and Auerbach, A. (2005) *Proc. Natl. Acad. Sci. U.S.A.* **102,** 15069–15074
25. Jha, A., Purohit, P., and Auerbach, A. (2009) *Biophys. J.* **96,** 4075–4084
26. Lee, W. Y., Free, C. R., and Sine, S. M. (2009) *J. Neurosci.* **29,** 3189–3199
27. Jha, A., Cadugan, D. J., Purohit, P., and Auerbach, A. (2007) *J. Gen. Physiol.* **130,** 547–558
28. Auerbach, A., Sigurdson, W., Chen, J., and Akk, G. (1996) *J. Physiol.* **494,** 155–170
29. Qin, F., Auerbach, A., and Sachs, F. (1996) *Biophys. J.* **70,** 264–280
30. Cadugan, D. J., and Auerbach, A. (2010) *Biophys. J.* **99,** 798–807
31. Cymes, G. D., Grosman, C., and Auerbach, A. (2002) *Biochemistry* **41,** 5548–5555
32. Chakrapani, S., and Auerbach, A. (2005) *Proc. Natl. Acad. Sci. U.S.A.* **102,** 87–92